

# High-intensity illumination treatments against LeTID – Intensity and temperature dependence of stability and inline feasibility

Henri Vahlman <sup>\*,1</sup>, Sebastian Roder <sup>1,\*\*</sup>, Jan Nekarda, Stefan Rein

Fraunhofer Institute of Solar Energy Systems ISE, Heidenhofstraße 2, 79110, Freiburg, Germany



## ARTICLE INFO

### Keywords:

Light- and elevated temperature-induced degradation (LeTID)  
High-intensity illumination treatment (HIIT)  
Regeneration  
Multicrystalline silicon (mc-Si)  
Industrial feasibility  
Solar cells

## ABSTRACT

We study the mitigation of light- and elevated temperature-induced degradation (LeTID) with high-intensity illumination treatments, placing special emphasis on inline feasibility. After the treatments, we investigate the stability upon degradation conditions close to the recently suggested standard, which allows estimating the LeTID behavior during the operating lifetime of solar modules in the field. Subsequently, we map the stability at different treatment intensities and temperatures achievable with an air-cooled tool. We show that, when applying short treatment times, the stability improves with increasing treatment intensity and deteriorates steeply with rising temperature above an optimum region around 250 °C. However, these intensity- and temperature-dependent differences largely vanish when increasing the treatment time sufficiently. We also investigate the significance of darkness/illumination during the cooling ramp from the treatment temperature in view of the LeTID stability. We discuss our results based on suggested defect models of LeTID, and provide hypotheses of the origin of the instabilities observed at the high treatment temperatures. After identifying optimal treatments, we demonstrate that the energy yield loss due to LeTID reduces by over 60% after an inline-feasible process consisting of only 30 s of high-intensity illumination, combined with cooling of the samples from the process temperature under a lower-intensity illumination.

## 1. Introduction

To achieve the full efficiency potential of passivated emitter and rear solar cells (PERC), it is important to suppress light-induced degradation (LID) mechanisms such as the boron-oxygen (BO) defect [1] and the so-called light- and elevated temperature-induced degradation (LeTID) [2–4]. Recently, effective methods to mitigate BO-LID in an inline-compatible timescale have emerged [5] while for LeTID no widely adopted inline solution exists. Although Cz-Si PERCs have also been found susceptible to LeTID [6], mc-Si PERCs can be particularly harmfully impacted with a relative power loss of up to 14% during the operating lifetime [7].

In solar modules, the degradation phase of LeTID lasts from several years to decades depending on the field location, and is followed by regeneration during which the efficiency recovers [2]. As shown by previous studies, LeTID cannot be explained by BO-, iron-boron- (FeB), or Cu-related LID [3,8]. Furthermore, LeTID also occurs in Ga-doped mc-Si and n-type wafers [3,9,10]. So far, the origin of LeTID is

unknown, although studies have postulated that hydrogen is closely involved in its formation [9,11–13].

To account for the degradation-regeneration behavior of LeTID, several different defect models have been proposed. At least three different states are necessary to explain the degradation and the following regeneration. These include an electrically inactive precursor that can change into the recombination-active degraded defect under illumination at elevated temperature. The subsequent recovery under illumination can be explained by a transformation of the recombination-active defect into the regenerated state. It is noteworthy that some experiments have necessitated the subdivision of the LeTID precursor state into two separate ones to explain observations of degradation in two stages with different time constants [14]. Recently, the first of these precursor states was hypothesized to consist of hydrogen–boron (H–B) pairs, whose dissociation under illumination at elevated temperature would result in the formation of hydrogen in its neutral charge state ( $H^0$ ) which alone or together with an unknown defect “X” would form the second precursor state [15]. After a subsequent formation of the

\* Corresponding author.

\*\* Corresponding author.

E-mail addresses: [henri.vahlman@ise.fraunhofer.de](mailto:henri.vahlman@ise.fraunhofer.de) (H. Vahlman), [sebastian.roder@ise.fraunhofer.de](mailto:sebastian.roder@ise.fraunhofer.de) (S. Roder).

<sup>1</sup> These authors contributed equally to this work.

degraded state, regeneration could then derive e.g. from defect passivation or out-diffusion of H to the wafer surfaces [9]. According to an alternative theory, the hydrogen-defect X compound could be formed already during firing [16]. Its subsequent reconfiguration and dissociation under illumination at elevated temperature would then be responsible for the first and the second degradation stage of the LeTID defect, respectively, while regeneration would occur upon out-diffusion of the species X from the bulk to the surfaces and extended defects.

In addition to the above-described basic transformations between the different defect states, also the existence of reverse reactions, especially from the degraded state back into a precursor state have been proposed to explain a partially reversible recovery behavior after dark/illuminated annealing [14,17,18], and the fact that increasing the temperature during a degradation-regeneration cycle increases the amplitude of LeTID during a following stability test at a lower temperature [19]. Interestingly, experiments involving an apparent increase of defect precursors upon dark annealing have also necessitated the introduction of a fourth state: a reservoir that releases new precursors at elevated temperatures considerably above the defect activation threshold temperature of LeTID [20]. According to the above-mentioned defect models of LeTID, this precursor reservoir could consist of either H<sub>2</sub> dimers that reconfigure into H–B pairs (i.e. the 1st precursor state) during dark annealing [15], or alternatively the reservoir could be composed of metallic precipitates of the defect X which dissolve during the anneal to form the defect precursor [16].

Recently, Sio et al. [21] suggested an alternative model to the reservoir theory that is still consistent with many types of complicated behavior of LeTID during light-soaking and dark-annealing experiments. Instead of a defect reservoir, they propose that experimental observations are explainable by two separate defect pathways that form under light soaking on the one hand and during dark annealing on the other hand. Within this theory, the defect formed and regenerated through the light-soaking pathway would obey a three-state reaction model with illuminated annealing driving the forward reactions and dark annealing the reverse reactions. Further, dark annealing would drive another separate defect reaction that, in accordance with many experiments, would result in degradation at a slower rate than the defect formed under light soaking. This separate defect formed through the dark-annealing pathway would also ultimately recover through defect removal/passivation, e.g. out-diffusion of hydrogen. Such hydrogen out-diffusion or other defect removal mechanism could also explain why sufficiently long dark anneals can lead to a significant reduction of LeTID during subsequent light soaking as observed in several studies [20–23].

Even if the origin and the defect mechanism of LeTID are not yet fully clear, there are several approaches to suppress the degradation significantly. For instance, adapted metallization firing profiles [23,24], anneal steps before or after firing [23,25–28] and high-intensity illumination treatments (HIIT) [25,29–31] have been proposed. Despite encouraging results with these methods, a widespread acceptance by the industry is still pending. Regarding a post-firing HIIT, studies using lifetime test structures have shown that the degradation-regeneration cycle can be accelerated to a timescale of minutes [25,30]. In addition, promising stability results of mc-Si PERC solar cells have been obtained with the HIIT method [29,31].

Within this work, we broaden the current understanding of HIIT against LeTID. We apply a wider temperature and illumination intensity range than in previous studies with a laser-based rapid thermal processing (RTP) oven using temperatures up to 430 °C and illumination intensities up to 150 kW/m<sup>2</sup>. Importantly, this is a temperature range that can still be considered relatively safe in terms of degradation of the fired front silver (Ag) contacts during HIIT, as post-firing anneal temperatures above 450 °C have previously been observed to be necessary for such degradation to occur to a significant extent [32]. Our emphasis is to study the feasibility of transferring the HIIT from the laboratory to an inline production environment. Therefore, we mainly use compressed

air for cooling, which is the simplest and the most straightforward cooling method implementable in an inline tool.

In addition to the temperature and the intensity during the actual HIIT, we also investigate how conditions during the cooling ramp from the process temperature, when the treatment illumination turns off, affect the results. For example, dark annealing has been shown to influence the time-dependent behavior of LeTID significantly [20,33,34] which could lead to a deterioration of LeTID stability if these effects are significant during the cooling ramp. To investigate this possibility, we compare different treatments by cooling the samples in the dark, by applying illumination during the cooling ramp, and by separately dark annealing samples after HIIT.

For stability testing of LeTID, we use conditions that are as close as possible to the recently suggested standard test for 1000 h [2]. This provides a close estimation of the losses that occur in the bulk material during the operating lifetime of modules installed in the field in climate conditions equivalent to Central Europe. Subsequently, we map the optimum combinations of treatment intensities and temperatures from the point of view of LeTID stability, and estimate energy yield benefits of the optimum processes. Our results provide guidelines for industrial adaptation of HIIT, as well as directions for further development of the method.

## 2. Experimental

In this study, we used 180 μm thick 1.8 Ω-cm p-type high-performance multi-crystalline silicon (HP mc-Si) wafers, originating from neighboring positions of the ingot. After saw-damage etching and an HNF-dip, the wafers were POCl<sub>3</sub> diffused to form an 85 Ω/sq. emitter. Subsequently, the wafers were chemically edge isolated resulting in phosphosilicate glass removal at the front and full removal of the emitter at the rear side. This was followed by a 6 nm thick Al<sub>2</sub>O<sub>3</sub> layer deposition on the rear side using a FAST-ALD tool. A MAIA PECVD system was then used to create SiN<sub>x</sub> layers of 75 nm and 150 nm thicknesses at the front and the rear side, respectively. The samples were fired at 850 °C set peak temperature, cut into quarters with a laser and characterized as implied open-circuit voltage (iV<sub>oc</sub>) samples.

A laser-based rapid thermal processing (RTP) oven with photon energy of 1.27 eV was used for the HIIT processes. The process heat was provided by the laser light itself without an additional heat source. For controlling the sample temperature independently of the illumination intensity, compressed air was applied from above the sample at a maximum velocity of 5.6 m/s (at sample plane), which was still sufficiently moderate not to push the sample out of its place under the laser or result in excessive sample breakage.

The process temperature during HIIT was monitored *in-situ* with a commercially available infrared (IR) camera. The emissivity of the studied samples was determined using the IR camera, a thermocouple, and a high-precision hotplate. The regeneration processes were performed by using the temperature value provided by the IR camera. Afterwards, a correction was done to the temperature value given by the IR camera as described in Ref. [35]. The necessity for this correction derives from a high concentration of excess carriers being present during the high-intensity regeneration process, which can distort the measured temperature value of the IR camera (plasmonic effects) compared to low-injection conditions during the calibration.

Time-temperature profiles of two example HIIT processes with respect to time are shown in Fig. 1. In the beginning of each process, a fast heat-up ramp of 1 s was applied by using a high illumination intensity of up to 240 kW/m<sup>2</sup>. After reaching the target temperature, the intensity was down-regulated to the target intensity and the temperature fine-adjusted with the air cooling. Unless otherwise stated in the text, after reaching the desired process duration, the light source was turned off with a simultaneous adjustment of the speed of the cooling air to its maximum velocity of 5.6 m/s.

Before the aforementioned HIIT processing, the samples were stored

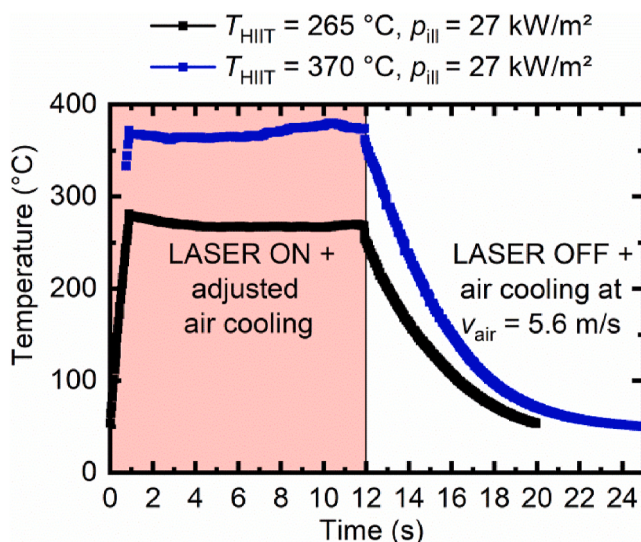


**Fig. 1.** Time–temperature profiles of the laser-based RTP oven at process temperatures of 265 °C (black) and 370 °C (blue) with a laser-on time of 12 s and an illumination intensity of 27 kW/m<sup>2</sup>. (For interpretation of the references to color in this figure legend, the reader is referred to the Web version of this article.)

in the dark for at least 48 h to ensure complete iron–boron (FeB) pairing [36]. These pairs were then dissociated with a high-intensity flash light, followed by the HIIT processes. After HIIT, a BO-degradation step was performed at 0.05 suns at room temperature (RT) for a minimum of 48 h to ensure that all remaining non-regenerated BO defects are in the degraded state. Afterwards, the FeB pairs were again dissociated with the high-intensity flash.

To test for LeTID, we applied 0.15 suns and 75 °C in open-circuit conditions. In terms of excess carrier concentration in the samples, these conditions are reasonably close to the recent module testing standard suggestion: operation at maximum power point under 1 sun at 75 °C [2].

Between the different experimental steps and time intervals of the LeTID test, lifetime measurements were performed using a quasi-steady-state photoconductance (QSSPC) equipment from Sinton instruments. To keep the analysis within the excess carrier concentration,  $\Delta n$ , range dominated by Shockley–Read–Hall recombination, all values of the effective lifetime,  $\tau_{\text{eff}}$ , are reported at a fixed  $\Delta n$  of  $0.1 \times N_A$ , where  $N_A$  is the acceptor dopant concentration.

A determination of the surface-related saturation current density,  $J_0$ ,<sub>surface</sub> was done according to the method introduced by Kimmerle et al. [37]. The  $\Delta n$  range for the fit varied from  $1 \times 10^{16}$  cm<sup>-3</sup> to  $2.5 \times 10^{16}$  cm<sup>-3</sup> depending on the interval where an unambiguous fit was obtainable.

### 3. Results and discussion

#### 3.1. LeTID behavior and surface-related dark saturation current density as a function of the duration of HIIT

One of the key factors of a process to be transferred inline is its duration. From the point of view of securing a sufficient throughput while minimizing the factory footprint of the inline tool, short processes in the order of tens of seconds are the most desirable. To study the significance of the treatment time,  $iV_{\text{oc}}$  samples were HIIT processed from 12 s to 3 min at a fixed intensity and temperature of 27 kW/m<sup>2</sup> and 265 °C, respectively. Subsequently, these samples were subjected to the LeTID test for 1000 h while monitoring the stability of  $\tau_{\text{eff}}$  (at  $\Delta n = 0.1 \times N_A$ ) with regular QSSPC-lifetime measurements. It is important to note that 1000 h of the suggested standard test conditions (which we

replicate) have been estimated to correspond to approximately a 20-year lifetime of field operation in the case of solar modules located in the Central European climate [2]. Hence, the results of the LeTID test, illustrated in Fig. 2, approximate the degradation expected during the majority of this operating lifetime.

Note in Fig. 2 that there are several measurement steps before the actual LeTID test, which from left to right correspond to  $\tau_{\text{eff}}$  in the FeB-paired state of impurity iron,  $\tau_{\text{eff}}$  after dissociation of these pairs to interstitial iron, Fe(i),  $\tau_{\text{eff}}$  immediately after HIIT, and  $\tau_{\text{eff}}$  after a subsequent degradation of the BO defect and dissociation of the FeB pairs.

Regarding the effect of the FeB pairs, it is noteworthy that their dissociation increases the effective lifetime by 6.7 μs on average (see FeB before HIIT vs. Fe(i) before HIIT). This effect is relatively small compared to the changes in the effective lifetime induced by the LeTID test conditions on the right side of Fig. 2, especially as this maximum effective lifetime variation by the FeB defects reduces considerably with the progress of the LeTID-related degradation (through the well-known  $1/\tau$  rule).

Importantly, all HIIT processes in Fig. 2 increase  $\tau_{\text{eff}}$  from its value before the treatment. In addition to recovery/regeneration of the BO defect, this increase may be at least partly related to so-called advanced hydrogenation which has been found to improve the effective lifetime after process steps at high intensities and temperatures [14]. It is noteworthy that the effects of the advanced hydrogenation are expected to remain stable during subsequent light soaking in both room temperature and LeTID test conditions [14].

When it comes to the BO defect, we note that based on an earlier study by Wilking et al., regeneration treatments as short as a few seconds at 250 °C and 2.7 suns are sufficient to bring practically all BO defects either into the regenerated state (majority of the defects) or the annealed state (minority of the defects) in 1.5 Ω·cm p-type Si [38]. The completeness of these transitions after 12 s of HIIT at 265 °C in our case is supported by the fact that the effective lifetime increases approximately by a similar amount both after HIIT for 12 s and for 3 min. A subsequent degradation due to BO-LID then reduces the effective lifetime by 1.6 μs on average in the HIIT-processed samples. In the case of the reference, a more pronounced degradation of the effective lifetime from 125 μs of the as-fired, FeB-dissociated state to 119 μs of the Fe(i) after BO-LID state can be observed which based on similar considerations as above for the FeB defect is still rather minor compared to the

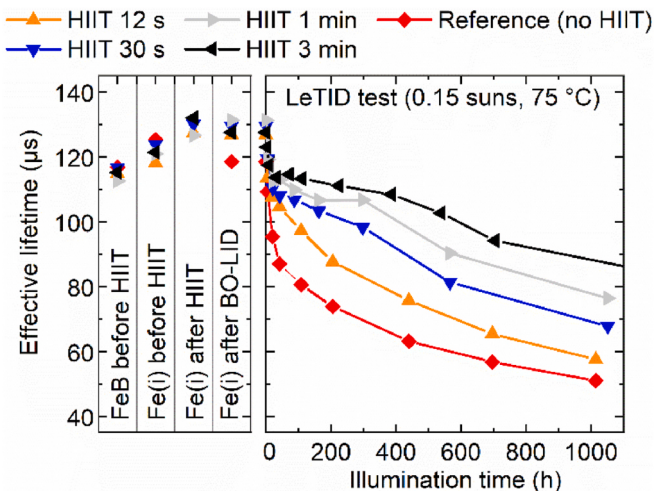


**Fig. 2.** Effective minority carrier lifetime (at  $\Delta n = 0.1 \times N_A$ ) after different HIIT-treatment times at 27 kW/m<sup>2</sup> and 265 °C as a function of the stability testing duration. The descriptions inside the figure signify the stage of the experiment and whether impurity iron is paired with dopant B (FeB) or whether these pairs are dissociated and iron exists as an interstitial atom Fe(i). The lines represent a linear interpolation between different experimental measurement points.

degradation during the LeTID test. Hence, we do not expect the BO defects any more than the FeB defects to play more than a relatively small role in the degradation observed during the LeTID test.

Moving to the right-hand side of Fig. 2 (the LeTID test), the samples show a consistently improving stability with increasing HIIT-treatment time, verifying the potential of HIIT in mitigating LeTID. This is also manifested in Table 1 by the decreasing drop of  $iV_{oc}$  during the 1000 h stability test with increasing treatment duration, from an average initial value of 669 mV. However, none of the treatment durations result in full stability during the LeTID test. Instead, an initial fast phase is followed by a slow gradual one in all cases in accordance with earlier results [29]. It is noteworthy that HIIT seems to reduce the initial fast stage of degradation especially strongly.

In addition to bulk degradation, several studies have reported changes in surface passivation quality originating from a possible surface-related degradation (SRD), induced by the LeTID test conditions applied in these studies [39,40]. In our case, the SRD could be induced either by the HIIT process, by the LeTID test, or by their combination. To study this possibility, we determined  $J_{0,surface}$  of the samples as described in Ref. [37]. Note that, in our case, the determined  $J_{0,surface}$  can be interpreted as the combined total  $J_0$  of both the  $\text{POCl}_3$ -diffused and  $\text{SiN}_x$ -coated front surface and the  $\text{Al}_2\text{O}_3/\text{SiN}_x$  stack on the rear surface [22,41].

The total surface-related saturation current density values,  $J_{0,surface}$ , of the samples of Fig. 2 are plotted in Fig. 3 at different stages of the experiment. These stages include the FeB-dissociated state before HIIT, the FeB-dissociated state after HIIT, and after applying the LeTID test for  $> 1000$  h. The results show insignificant changes of  $J_{0,surface}$  for all of the samples both after the HIIT process and after the LeTID test. Hence, the changes of the effective lifetime in Fig. 2 are very likely attributable to bulk defects.

The short treatments in Fig. 2 result in only partial stabilization at  $27 \text{ kW/m}^2$  and  $265^\circ\text{C}$ . Therefore, stability at other possible treatment intensities and temperatures becomes a relevant question. Hence, we will proceed below by investigating if the stability improves by varying the intensity and/or the temperature within the operating range of the tool. In the next section, to facilitate this goal, we define a useful measure of stability to promote a clear comparison of a large number of different HIIT processes.

### 3.2. Time integral of normalized defect concentration as a measure of stability

To ease the comparison of stability test results of various HIIT processes, we define a figure of merit for the stability of the  $iV_{oc}$  samples. As full stability was not reached with the treatments of Fig. 2, our approach with the mentioned figure of merit is that it should be able to evaluate whether applying HIIT would reduce or increase LeTID-related losses during a testing timespan correlatable to a typical field operating lifetime of solar modules. In addition, it should be able to evaluate qualitative differences in the effectiveness of different HIIT processes at various temperatures and intensities (i.e., whether one treatment is better than another one). Here, we assume that the LeTID-related power loss is proportional to the concentration of active LeTID defects in the sample, which can be quantified by calculating the so-called normalized defect concentration,  $N^*$ , as will be described below [1]. We also

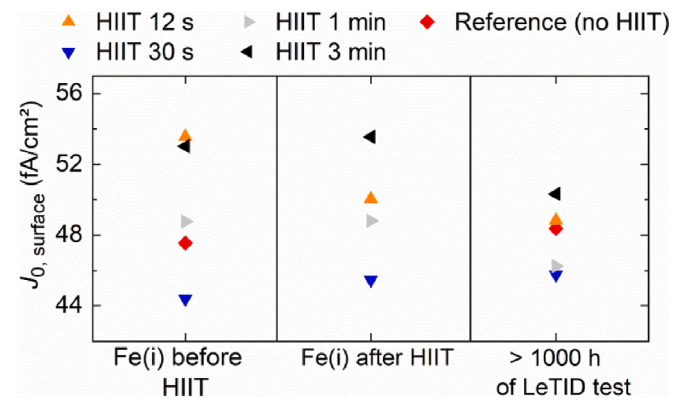


**Fig. 3.** Surface-related saturation current density  $J_{0,surface}$  (fit range of  $\Delta n$  was between  $1 \times 10^{16} \text{ cm}^{-3}$  and  $2.5 \times 10^{16} \text{ cm}^{-3}$ ) for the different stages of the LeTID test: FeB-dissociated state before HIIT, FeB-dissociated state after HIIT, and after  $> 1000$  h of LeTID testing. Note that the  $J_{0,surface}$  values were determined from the same samples as shown in Fig. 2.

consider that the energy yield losses of solar cells due to light-induced defects are proportional to the time spent in each specific phase of degradation, quantified by  $N^*$ . Therefore, we base our figure of merit of stability on time integration of  $N^*$  across the 1000 h LeTID testing time.

The concentrations of light-induced defects in different samples with varying initial lifetimes can be compared directly by calculating  $N^*$  as

$$N^* = \frac{1}{\tau_{\text{eff}}(t)} - \frac{1}{\tau_{\text{Fe}(i) \text{ before HIIT}}}, \quad (1)$$

where  $t$  is the LeTID testing time,  $\tau_{\text{Fe}(i) \text{ before HIIT}}$  is the minority carrier lifetime before HIIT in the FeB dissociated state, and both  $\tau_{\text{eff}}(t)$  and  $\tau_{\text{Fe}(i) \text{ before HIIT}}$  are evaluated at the same fixed  $\Delta n = 0.1 \times N_A$  [1]. After defining  $N^*$  with Eq. (1), we take its time integral from 0 h to 1000 h as

$$N^* = \int_{0 \text{ h}}^{1000 \text{ h}} N^*(t) dt. \quad (2)$$

**Fig. 4** illustrates  $N^*$  as defined by Eq. (1) for a sample treated for 3 min at  $27 \text{ kW/m}^2$  and  $265^\circ\text{C}$  as well as for a non-treated reference. The

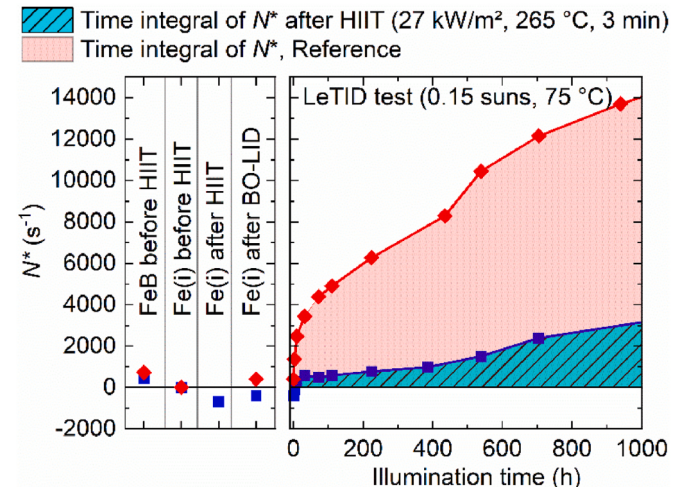


**Fig. 4.** Normalized defect concentration,  $N^*$ , of LeTID-related defects (at  $\Delta n = 0.1 \times N_A$ ) as a function of the LeTID testing time. Note that the shaded areas, i.e. the time integrals of  $N^*$ , are used below as a figure of merit of the stability of different HIIT processes. The descriptions inside the figure signify the stage of the experiment and whether impurity iron is paired with dopant B (FeB) or whether these pairs are dissociated and iron exists as an interstitial atom (Fe(i)).

**Table 1**

Average loss of  $iV_{oc}$  during the 1000 h LeTID test after HIIT of different durations at  $27 \text{ kW/m}^2$  and  $265^\circ\text{C}$ . Note that the average is based on 4 samples in the case of the references and the 12 s HIIT, one sample in the case of the 30 s and the 1 min HIIT, and two samples in the case of the 3 min HIIT.

Treatment time	Ref. (0 s)	12 s	30 s	1 min	3 min
$iV_{oc}$ loss after 1000 h	31.3 mV	25.9 mV	18.9 mV	14.7 mV	12.9 mV

time integral according to Eq. (2) is visible as the area between  $N^*$  and the illumination time-axis.

As stated above in conjunction with Fig. 2, the FeB and the BO defects have only a relatively minor role compared to the light-induced effects that occur in the LeTID test conditions. This can also be seen on the left side of Fig. 4, illustrating the effect of the associated experimental steps on  $N^*$ . Further, the results of Fig. 3 strongly imply that the surface passivation quality stays stable during the experiments. Therefore, we expect all changes in  $N^*$  that occur during the LeTID test to reliably reflect the concentration of the LeTID defects in the bulk of the samples [42].

It is noteworthy in Eq. (1) that, by normalizing  $N^*$  with respect to  $\tau_{\text{Fe(i)}}$  before HIIT, it includes both the changes in the sample during HIIT and those activated by the LeTID test. Hence, it is also affected by the slight increase in lifetime upon HIIT, which is possibly influenced by advanced hydrogenation as discussed above in Sec. 3.1. Although the fact that  $N^*$  may be influenced by phenomena not directly associated with LeTID (i.e. BO recovery/regeneration and/or advanced hydrogenation) is not ideal, normalization of  $N^*$  to an effective lifetime value after HIIT is not a good option either since this approach would ignore possible LeTID activation during HIIT. However, as shown in Fig. 4, the effect of the effective lifetime increase upon HIIT has a relatively small impact on  $N^*$  as compared to the changes during the LeTID test. Therefore, the time integral of  $N^*$  can be interpreted as a reasonably reliable measure of instability due to the LeTID defect, which takes into account the different phases of degradation throughout the entire 1000 h of LeTID testing time.

### 3.3. Immediate impact of HIIT on $N^*$

To ensure the relevance of the results for inline applications, we chose the short 12 s process time as the shortest duration with which to apply a wide variation of temperatures and illumination intensities during HIIT. Our main motivation for studying HIIT durations as short as 12 s is to investigate the LeTID stability improvement achievable with an inline tool with a high throughput, yet a small factory footprint. In a simplified example where a requirement of industrial throughput of 4000 wafers/hour together with the process duration and a gap of 0.2 times the sample length between individual cells defines the minimum length of the laser chamber, HIIT of 12 s would require a laser chamber that is 2.5 m long, whereas for a 30 s process the chamber length has to be increased to 6.2 m. In addition to the 12 s HIIT addressed here, we also study longer processes of 30 s, 60 s, 3 min, and 10 min in later sections.

The tested illumination intensities and temperatures of this study cover the reachable parameter range of our air-cooling-based laser treatment setup. This range is illustrated in Fig. 5, together with a single intensity–temperature combination marked with a star symbol, which was obtained by using water cooling to see if notable benefits are achievable at intensities above the air-cooled range. Regarding the process temperature limits of HIIT, it is also important to note that increasing the temperature too much may risk damaging the fired Ag metallization of full solar cells. For example, Chan et al. showed that post-firing anneals at and above 450 °C for 180 s degrade the contacts significantly, whereas similar processes at lower temperatures (e.g. at 400 °C) do not result in a notable degradation [32]. This increase of the contact resistance was attributed both to the motion of charged particles such as hydrogen to the area occupied by the contacts and a change in the structure of the Ag–Si interface. To support these observations, inline HIIT at 400 °C was recently observed to be benign for the efficiency of mc-Si PERC solar cells implying negligible damage to the contacts, whereas increasing the temperature to 450 °C resulted in an efficiency loss immediately after the treatment that could be a sign of high-temperature-induced degradation of the contact resistance [43]. Hence, we chose not to exceed 430 °C HIIT temperature in the present

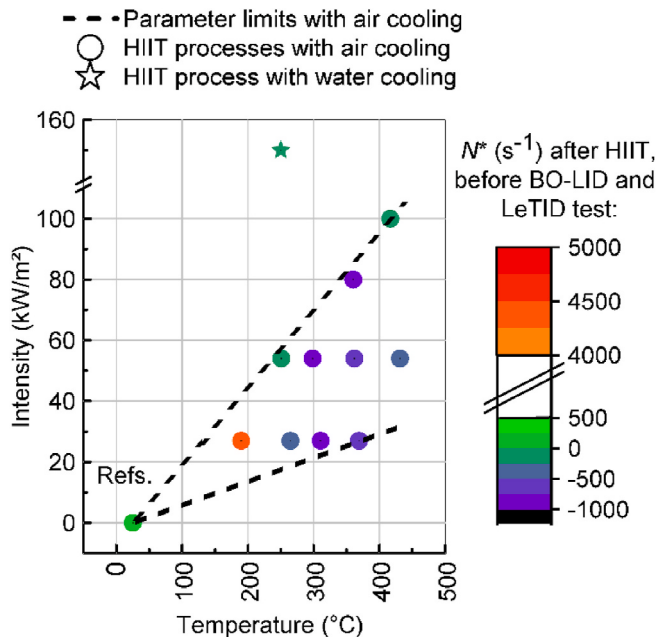


**Fig. 5.** Average normalized defect concentration,  $N^*$ , (at  $\Delta n = 0.1 \times N_A$ ) after 12 s HIIT at different intensities and temperatures in the Fe(i) state before BO-LID. The dashed lines indicate the achievable intensity and temperature combinations with velocity of the cooling air between 0 and 5.6 m/s. Most processes were performed using air cooling, except for one water-cooled process at 150 kW/m<sup>2</sup> and 250 °C, marked with a star symbol. At least two samples were processed per parameter combination. Note that the slight differences between the temperatures between the treatments at different intensities derive from the intensity dependence of the temperature correction of the IR camera as described in the experimental section.

study.

Before proceeding to the results of the LeTID test, it is relevant to illustrate the immediate impact of different HIIT processes on  $\tau_{\text{eff}}$ , and therefore  $N^*$ . The color scale of Fig. 5 depicts the average  $N^*$  (of at least two samples) immediately after 12 s HIIT, before BO-LID. Note that the small shifts in the treatment temperatures in the case of treatments at different intensities derive from the intensity-dependent temperature correction as described in the experimental section.

The results of Fig. 5 show that  $N^*$  changes only marginally during most of the HIIT processes, and in most cases the change of  $N^*$  is negative (i.e. the effective lifetime increases). The only exception is the process at 27 kW/m<sup>2</sup> and 190 °C, which leads to a considerable increase of  $N^*$ . This result can be reflected based on Ref. [44] which reported that HIIT at and below 200 °C leads to a degradation–regeneration cycle of  $\tau_{\text{eff}}$  in symmetric HP mc-Si lifetime samples, whereas temperatures higher than this result in a monotonous increase of  $\tau_{\text{eff}}$  (i.e. decrease of  $N^*$ ). In Ref. [44], the duration of this cycle was ~90 s at 30.5 kW/m<sup>2</sup> and 200 °C. Hence, the increased  $N^*$  may derive from an unfinished LeTID cycle after 12 s of HIIT at 27 kW/m<sup>2</sup> and 190 °C.

To verify the above-mentioned HIIT temperature-dependent differences with our  $iV_{\text{oc}}$  samples, Fig. 6 illustrates the effective lifetime as characterized with the QSSPC method (at  $\Delta n = 0.1 \times N_A$ ) every few seconds during the course of two different HIIT processes: at 14 kW/m<sup>2</sup> and 190 °C and at 17 kW/m<sup>2</sup> and 265 °C. Note here, that a short high-intensity pulse of 270 kW/m<sup>2</sup> of a few hundred milliseconds was necessary at the start of each HIIT interval to increase the sample temperature quickly to the target temperature, after which the intensity was adjusted down to the values indicated in the figure. After each treatment interval, the sample was air cooled and measured at the room temperature. Overall, Fig. 6 provides qualitatively similar results as Ref. [44]: Whereas a clear degradation–regeneration cycle that lasts up to several

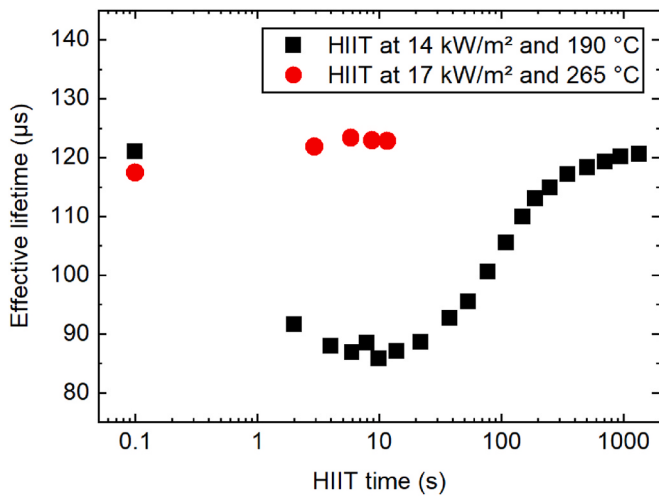


**Fig. 6.** Effective minority carrier lifetime during the course of HIIT in the case of two different processes: at  $14 \text{ kW/m}^2$  and  $190^\circ\text{C}$  and at  $17 \text{ kW/m}^2$  and  $265^\circ\text{C}$ . Note that at the start of each HIIT phase, a short high-intensity pulse at  $270 \text{ kW/m}^2$ , with a duration of a few hundred milliseconds was applied to heat the sample up quickly to the process temperature, after which the intensity was adjusted to the target intensity denoted in the legend. After each treatment interval, the sample was air cooled and measured at the room temperature with the QSSPC method (at  $\Delta n = 0.1 \times N_A$ ).

minutes occurs during the treatment at  $190^\circ\text{C}$ , no degradation but only a slight monotonous increase of the effective lifetime is visible in the case of the treatment at  $265^\circ\text{C}$  instead.

Based on the above considerations, we can conclude that the 12 s treatment at  $190^\circ\text{C}$  in Fig. 5 is not enough to bring the sample fully through the typical LeTID cycle, which leaves  $N^*$  high at the end of the process. On the other hand, as also seen in other studies above a certain threshold temperature [19,44], it is likely that a visible degradation-regeneration sequence does not occur at all during any of the other processes of Fig. 5. This may derive from the acceleration of the lifetime-increasing reaction (e.g. regeneration) with increasing temperature so that it becomes considerably faster than the degradation reaction beyond  $\sim 250^\circ\text{C}$ .

#### 3.4. Optimum LeTID mitigation with short 12 s HIIT

After application of the different HIIT processes shown in Fig. 5, the samples were tested for LeTID. Fig. 7 illustrates the stability with the average time integral of  $N^*$  from 0 h to 1000 h (see Eq. (2)), as functions of HIIT temperature and intensity. To reduce the impact of possible outliers, at least two samples per process condition were characterized. To improve the evaluation of whether a process leads to a reduction or an increase in the overall impact of LeTID, we have adopted in the following text a convention of normalizing the time integrals of  $N^*$  by dividing them with the average value of the time integrals of  $N^*$  of five non-treated references. This means that, based on the considerations presented in detail in Sec. 3.2, HIIT processes with values  $< 1$  improve the stability, whereas processes with values  $> 1$  reduce the stability. Note that although only average values of the time integrals of  $N^*$  are reported in Fig. 7, also individual values for each sample (on which the averages are based upon) are available and are shown below in Fig. 8 of Sec. 3.5 in a 3D-plot.

Among the air-cooled samples within the dashed lines in Fig. 7, the HIIT at  $52 \text{ kW/m}^2$  and  $250^\circ\text{C}$  results in the lowest time integral of  $N^*$ . This optimum deteriorates when moving to a lower intensity at  $27 \text{ kW/m}^2$  and  $265^\circ\text{C}$ . We consider it likely that the majority of this difference derives from the considerable change in the treatment intensity, although these processes also have a modest relative difference in

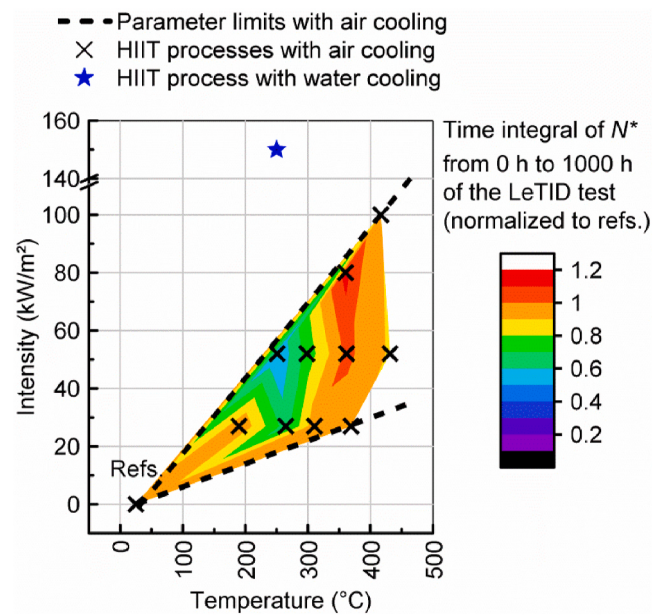


**Fig. 7.** Average time integral of the normalized defect concentration,  $N^*$ , from 0 h to 1000 h based on the LeTID test, after a 12 s HIIT at different intensities and temperatures. Note that all values of the average time integral of  $N^*$  were normalized by dividing with the average value of the time integrals of  $N^*$  of five non-treated references. At least two samples were tested per parameter combination (note that the time integral of  $N^*$  for each individual sample is further illustrated below in Fig. 8 with a 3D-plot). Dashed lines indicate the achievable intensity and temperature combinations with velocity of the cooling air between 0 and  $5.6 \text{ m/s}$ . The contour levels were calculated by linear interpolation. In addition, the star depicts a single point processed using water cooling, and is color coded according to the contour levels of the rest of the figure. (For interpretation of the references to color in this figure legend, the reader is referred to the Web version of this article.)

temperature by less than 3% in the absolute scale (originating from the intensity-dependent temperature correction).

Based on Fig. 7, the optimum temperature for the 12 s processes is around  $250^\circ\text{C}$ . Moving to a lower temperature of  $190^\circ\text{C}$  while keeping the intensity constant at  $27 \text{ kW/m}^2$  results in an increase in the time integral of  $N^*$  to values similar to the references. This increase derives largely from the fact that, as illustrated in Fig. 5,  $N^*$  is very high already at the end of the  $190^\circ\text{C}$  HIIT process, before the LeTID test. More unexpectedly, however, the time integral of  $N^*$  deteriorates considerably also with increasing temperature. For instance, there is no clear difference in the time integral of  $N^*$  between the samples treated at or above  $360^\circ\text{C}$  and the references. At the high temperatures, the time integral of  $N^*$  does not decrease even after increasing the intensity to very high values between  $80 \text{ kW/m}^2$  and  $100 \text{ kW/m}^2$ .

At the optimum temperature around  $250^\circ\text{C}$ , the stability seems to improve promisingly toward higher intensities. Therefore, we used a water-cooled chuck to investigate the further potential of the HIIT method at a very high intensity not achievable with air cooling around this temperature range. As depicted by the star symbol, colored in accordance with the contour levels of Fig. 7, the time integral of  $N^*$  decreases considerably when increasing the intensity from  $52 \text{ kW/m}^2$  to  $150 \text{ kW/m}^2$ . This suggests that liquid cooling could be beneficial in terms of LeTID stabilization also in an inline system despite a more complicated structure and therefore a higher cost compared to air cooling. Note that the practical benefits from these treatments in terms of expected reduction of energy yield loss and degradation of implied  $V_{oc}$  due to LeTID are evaluated below in Sec. 3.9.

Regarding qualitative time-dependent degradation characteristics

(not visible in Fig. 7), we note that all illustrated samples behaved similarly during the 1000 h LeTID test as the samples of Fig. 2: After a fast initial degradation there was a slow gradual degradation phase without visible regeneration during the testing time. In addition, similar to Fig. 3 in the case of HIIT at 265 °C, no increase of  $J_{0,surface}$  and therefore SRD occurred at any stage of the experiments even after the highest temperature HIIT processes above 360 °C (data not shown). Note that although these considerations apply also to all other treatments reported later in this study, we cannot exclude the possibility of bulk regeneration and/or SRD substantially beyond 1000 h in the LeTID test conditions of this work. We also cannot rule out the possibility that, if such a regeneration were to occur, the non-treated references would start regenerating earlier than the HIIT-processed samples such as was observed in a previous study [31]. Hence, the conclusions of this work are mainly limited to field conditions that are approximately equivalent to Central Europe (see section 3.1), and are not necessarily generalizable to considerably warmer climates.

### 3.5. Treatment time dependence of LeTID stability after HIIT at different intensities and temperatures

To gain more understanding on treatment intensity and temperature dependence of stability, the air-cooled HIIT process was prolonged to 3 min for a set of samples. Fig. 8 compares the time integral values of  $N^*$  of the 3 min treatments to the air-cooled 12 s treatments of Fig. 7. Note that, to obtain a clear visualization, the plot was smoothed with a total points increase factor of 100 and a smoothing parameter of 0.05 of ORIGIN 2019 software [45]. Further, the red, the blue, and the green spheres illustrate the time integral of  $N^*$  in the case of individual samples corresponding to the 12 s HIIT processes, the 3 min HIIT processes, and the non-treated references, respectively.

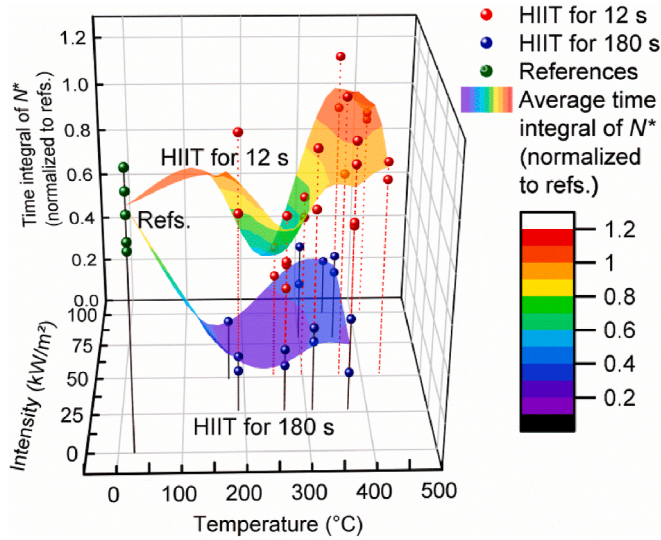


**Fig. 8.** Time integral of normalized defect concentration,  $N^*$ , from 0 h to 1000 h of LeTID testing after HIIT-processing times of 12 s and 3 min at different intensities and temperatures. All values of the time integral of  $N^*$  were normalized by dividing with the average value of the time integrals of  $N^*$  of five non-treated references. The red, the blue, and the green spheres illustrate individual values of the time integral of  $N^*$  of samples corresponding to 12 s HIIT, 3 min HIIT, and the references, respectively. Note that the data for the 12 s HIIT are the same as Fig. 7 is based on. To clarify the illustration, the average contours were smoothed with a total points increase factor of 100 and a smoothing parameter of 0.05 of ORIGIN 2019 software [45]. (For interpretation of the references to color in this figure legend, the reader is referred to the Web version of this article.)

The results of Fig. 8 show that prolonging the treatment time from 12 s to 3 min improves the stability considerably at all of the temperature and intensity combinations. Unlike in the case of the 12 s HIIT, a considerable reduction of LeTID compared to the references results even when increasing the temperature of the 3 min treatments above 300 °C. Another difference compared to the 12 s processes is that also the processes around 190 °C become useable when the treatment time increases to 3 min. This derives most likely from the fact that, unlike the 12 s HIIT, the 3 min treatment provides enough time to cycle through the full degradation–regeneration cycle of LeTID (see the discussion in section 3.3).

Curiously, in Fig. 8, there is a considerably wider gap of stability between the 12 s and 3 min HIIT at high temperatures above 300 °C than at the optimum temperature around 250 °C. To investigate this further, we included two additional treatment times, 30 s and 1 min, at 27 kW/m<sup>2</sup> and two different temperatures: 265 °C and 370 °C. In addition, HIIT at 27 kW/m<sup>2</sup> and 265 °C was continued 10 min with a pair of samples. Fig. 9 shows the results as the time integral of  $N^*$ , normalized to the references as above, as a function of the HIIT-process time. Also shown for comparison are the time integrals of  $N^*$  of the optimum air-cooled and water-cooled processes from Fig. 7 at 52 kW/m<sup>2</sup> and 150 kW/m<sup>2</sup>, respectively, both at 250 °C for 12 s.

At short treatment durations of 12–60 s, the results of Fig. 9 indicate a better stability for the 27 kW/m<sup>2</sup> HIIT process at 265 °C than at 370 °C. However, the treatments at both temperatures consistently approach a similar value of the time integral of  $N^*$  at a treatment time of 3 min.

Unintuitively, the higher-temperature treatment at 27 kW/m<sup>2</sup> and 370 °C in Fig. 9 approaches the apparent common saturation value slower than the lower-temperature treatment at 27 kW/m<sup>2</sup> and 265 °C. As a counterexample, the regeneration rate of LeTID has been shown to follow Arrhenius-type kinetics leading to increasing regeneration rate with increasing temperature, although this evaluation was limited to

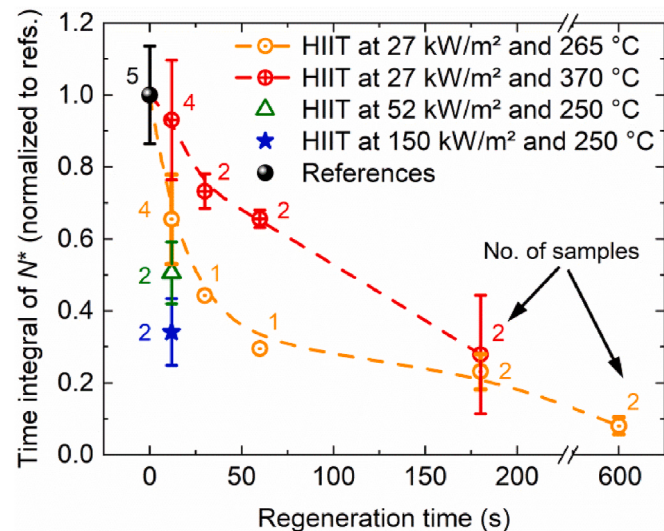


**Fig. 9.** Average time integral of normalized defect concentration,  $N^*$ , from 0 h to 1000 h of LeTID testing after HIIT processes of different durations at 27 kW/m<sup>2</sup> and both 265 °C and 370 °C as a function of the HIIT-treatment duration. All values of the time integral of  $N^*$  were normalized by dividing with the average value of the time integrals of  $N^*$  of five non-treated references. Included for comparison are the air- and water-cooled 12 s HIIT processes from Fig. 7 at 52 kW/m<sup>2</sup> and 250 °C (air cooled, green triangle), and at 150 kW/m<sup>2</sup> and 250 °C (water cooled, blue star), respectively. Note that the number of samples used for each experimental condition is illustrated next to the average points. The error bars indicate the sample standard deviation when several samples were characterized and the lines serve as guides to the eye. (For interpretation of the references to color in this figure legend, the reader is referred to the Web version of this article.)

temperatures below 200 °C [44]. Nevertheless, qualitatively similar results to Fig. 9 were also observed by Payne et al. [29], who found that increasing the temperature of a short HIIT from 200 °C to 250 °C reduced the stability of mc-Si solar cells, while prolonging the process time to minutes improved the stability at both temperatures.

In principle, the above complicated temperature dependence of the LeTID stability after HIIT could be influenced not only by the treatment intensity and temperature themselves, but also by the short dark-annealing period when the illumination turns off at the end of the process (see Fig. 1). Therefore, before proceeding in section 3.7 to further interpretation of the results of Figs. 7–9, we investigate the relative significance of the conditions during the cooling ramp in the following section (Sec. 3.6).

### 3.6. Effect of dark annealing and illumination during cooling ramp of HIIT

To examine the role of conditions during the cooling ramp from the process temperature of HIIT, we first remove the dark anneal by applying illumination also upon the cooling phase. Here, we use a low intensity of 1.5 kW/m<sup>2</sup> during cooling to achieve the same time-temperature profile as in Fig. 1 for the HIIT process at 27 kW/m<sup>2</sup> and 370 °C. We apply this illumination until the temperature of the samples reaches 60 °C, amounting to 15 s. For comparison, we also apply the same post-process illumination profile after other HIIT processes.

Fig. 10 shows a comparison of the time integral of  $N^*$  from 0 h to 1000 h of LeTID testing (normalized to the references as above) between samples that went through either cooling in the dark (left side of the figure) or under illumination (right side of the figure). The comparison includes three types of air-cooled processes applied before the cooling ramp, numbered from 1 to 3. Processes 1 and 2 are the same 27 kW/m<sup>2</sup> processes at 265 °C and 370 °C, respectively, as already shown above e.g. in Fig. 9. Process 3 consists only of the 1 s heat-up pulse of process 2, without the remaining 11 s period of constant illumination and temperature.

Comparing the left and the right side of Fig. 10, illumination during the cooling ramp improves the stability of both processes 1 (at 265 °C)

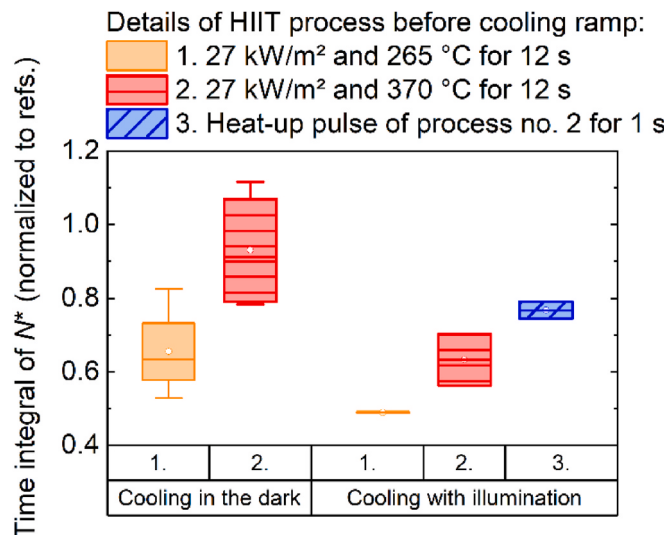


**Fig. 10.** Time integral of the normalized defect concentration,  $N^*$ , from 0 h to 1000 h of LeTID testing for differently HIIT-processed samples with and without illumination (1.5 kW/m<sup>2</sup>) during the cooling ramp from the process temperature down to 60 °C. The results are based on four samples per process for the samples cooled in the dark, and two samples per process for the samples cooled under illumination. All values of the time integral of  $N^*$  were normalized by dividing with the average value of the time integrals of  $N^*$  of five non-treated references.

and 2 (at 370 °C). Further, the stability improvement is clearly greater for the higher-temperature process at 370 °C. At this stage, there seems to be three options for the cause of this stability improvement. The first option is that, during the cooling ramp in the dark, the occurrence of destabilizing phenomena leads to a deterioration of the stability achieved with the preceding HIIT process. The second possibility is that the illuminated cooling ramp by itself provides favorable conditions for the forward reaction of LeTID regeneration, which improves the stability of the samples. As a third option, both options one and two contribute to the results of Fig. 10 together.

In Fig. 10, it is noteworthy that also applying solely the heat-up pulse of the 370 °C process and then illumination during cooling (i.e. process no. 3) improves the stability notably compared to the references. In this case, due to the shortness of the heat-up pulse (1 s), it appears likely that the majority of the stability improvement during process no. 3 would result from the illuminated cooling phase for 15 s. Although this result provides suggestive evidence that additional regeneration may occur during the illuminated cooling ramp (i.e. option two above), it does not exclude the possibility of destabilizing effects during the cooling ramp in the dark (i.e. option one).

In an attempt to reproduce the effects of the cooling ramp in the dark from the process temperature of 370 °C, we evaluate the impact of a separate short dark anneal after HIIT on LeTID stability. For this, we dark annealed two samples, originally processed at 52 kW/m<sup>2</sup> and 250 °C for 12 s, on a hotplate at 320 °C for 20 s. The  $N^*$  of one of these samples as a function of the LeTID test time is compared in Fig. 11 to a similarly HIIT-processed sample without a separate dark anneal. In addition, the time-dependent  $N^*$  curves for samples HIIT processed at 52 kW/m<sup>2</sup> and 300 °C for 12 s, at 52 kW/m<sup>2</sup> and 370 °C for 12 s, and a non-treated reference are shown for comparison. Although the temperature of the separate dark anneal is lower than the peak temperature while cooling from 370 °C, due to its longer duration we consider this treatment a reasonable upper-limit estimate to the effects of the cooling ramp from 370 °C to room temperature in the dark (during cooling, the temperature decreases from 370 °C to 320 °C within only 0.7 s, see Fig. 1).

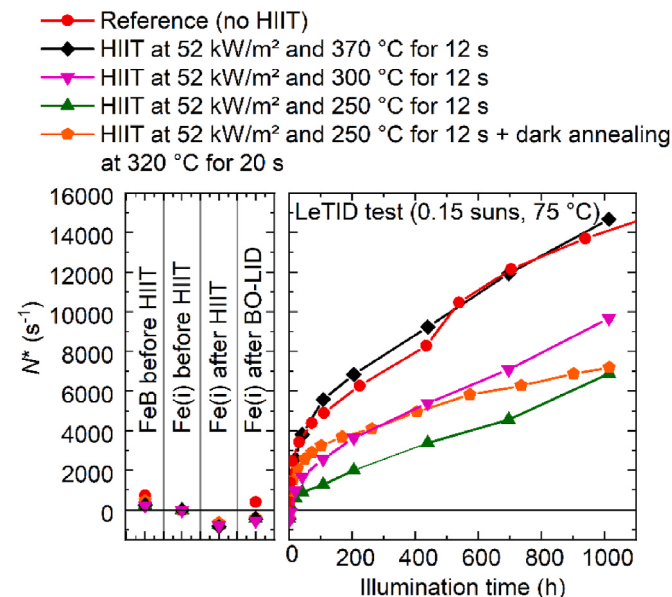


**Fig. 11.** Normalized defect concentration,  $N^*$ , as a function of the LeTID testing time after HIIT processes at 52 kW/m<sup>2</sup> and 250 °C, 300 °C, and 370 °C for 12 s. One sample type, first treated at 52 kW/m<sup>2</sup> and 250 °C for 12 s, was separately dark annealed for 20 s at 320 °C. Further, the figure shows  $N^*$  of a non-treated reference for comparison. Note that although the figure illustrates only one sample of each type, at least two similarly treated samples were characterized per sample type, and consistent trends observed in each case.

In Fig. 11, the sample that first experienced HIIT at  $52 \text{ kW/m}^2$  and  $250^\circ\text{C}$  for 12 s and then a separate dark anneal at  $320^\circ\text{C}$  for 20 s shows more degradation especially in the beginning of the LeTID test (during the first 100 h) compared to the similarly HIIT-processed sample without the separate dark anneal. This change is likely due to changes in the bulk of the samples, as the total  $J_{0,\text{surface}}$  of both sample types stayed constant during the experiments (data not shown, equivalent to Sec. 3.1). Hence, even a short dark anneal after HIIT may lead to visible changes in the bulk degradation behavior during a subsequent LeTID test. This type of change in the bulk behavior of LeTID is in qualitative agreement with earlier studies [25,34], and resembles a recent observation of Sio et al. [21] that a dark anneal at  $300^\circ\text{C}$  for 1 min leads to an increased normalized defect concentration during the course of a following light soaking. It is also noteworthy that  $N^*$  of the mentioned sample that was separately dark annealed at  $320^\circ\text{C}$  after HIIT overlaps quite closely with the sample that experienced HIIT at a temperature close to the dark-annealing temperature, at  $52 \text{ kW/m}^2$  and  $300^\circ\text{C}$  for 12 s. We discuss the possible reasons of this overlap further below in section 3.7.

Can the cooling ramp in the dark explain the stability differences between the short (e.g. 12 s) HIIT processes at  $265^\circ\text{C}$  on the one hand and at  $370^\circ\text{C}$  on the other hand in Fig. 9? As discussed above in conjunction with Fig. 11, we consider the separate dark anneal at  $320^\circ\text{C}$  for 20 s to provide a reasonable upper-limit estimate for the effects of the cooling ramp in the dark from the HIIT temperature of  $370^\circ\text{C}$  (due to the longer duration of the separate dark anneal compared to the cooling ramp in the dark, see Fig. 1). When applied after HIIT at  $52 \text{ kW/m}^2$  and  $250^\circ\text{C}$ , this separate dark anneal increases the amount of degradation during the LeTID test to some extent compared to the similarly HIIT-processed sample without the separate dark anneal (see Fig. 11), but the overall amplitudes of LeTID are still rather close to each other between these two sample types. On the other hand, the amplitude of LeTID after the high-temperature HIIT at  $52 \text{ kW/m}^2$  and  $370^\circ\text{C}$  in Fig. 11 is considerably greater than after HIIT at  $52 \text{ kW/m}^2$  and  $250^\circ\text{C}$  regardless of whether the separate dark anneal is performed after the lower-temperature HIIT or not. This result implies that, rather than destabilization due to dark annealing during the cooling ramp in the dark, the improvement of stability observed after illuminated cooling compared to cooling in the dark in Fig. 10 is more likely related to other phenomena such as additional regeneration during the illuminated cooling ramp. Importantly, it also means that dark annealing during the cooling ramp is unlikely to destabilize the samples sufficiently to explain the stability difference between the low- and the high-temperature HIIT in Fig. 11 ( $250^\circ\text{C}$  vs.  $370^\circ\text{C}$ ) and in Fig. 9 ( $265^\circ\text{C}$  vs.  $370^\circ\text{C}$ ) fully.

### 3.7. Interpretation of the process temperature dependence of HIIT based on defect models of LeTID

As the results of section 3.6 imply only a minor impact by dark annealing upon the cooling ramp, the instabilities observed in Figs. 7–9 after short HIIT at high temperatures  $> 300^\circ\text{C}$  relate likely to changes that the treatment temperature itself causes to the subsequent defect reactions during the LeTID test. In addition, the total  $J_{0,\text{surface}}$  stayed constant throughout the experiments (implying the absence of surface-related degradation), which suggests that these changes are imposed on the bulk LeTID defect. One explanation, based on a simple 3-state model, could be that the rate of a reverse reaction from the regenerated state back to one of the precursor states increases with increasing temperature. This could explain why a short HIIT (12 s–60 s) at  $370^\circ\text{C}$  in Fig. 9 results in more degradation than HIIT at  $265^\circ\text{C}$ . However, the increased rate of the reverse reactions should also influence the equilibrium concentrations of defects in the regenerated state on the one hand and in the precursor state(s) on the other hand. Therefore, the fact that the treatments at both  $370^\circ\text{C}$  and  $265^\circ\text{C}$  approach a similar stability when the process time extends to several minutes is more difficult

to fit in this picture. This implies that the three-state model may not be the correct one to explain the complicated temperature dependence of HIIT, and hence also other options should be looked into.

Another alternative, involving an additional reservoir state and the omission of the reverse defect reactions according to the 4-state model suggested by Fung et al. [20], would be that HIIT at  $300^\circ\text{C}$  and above promotes a release of precursors from the reservoir much more than HIIT at  $250^\circ\text{C}$ . Even if regeneration occurs at  $300^\circ\text{C}$  and above, the release of new precursors from the reservoir is equal in speed or faster compared to the regeneration reaction. Therefore, the stability improves considerably only after the reservoir depletes or equilibrates with the precursor states sufficiently and the rate of new precursor creation slows down. In the case of Fig. 9, this would require several minutes of HIIT at  $370^\circ\text{C}$ , after which the remaining precursors would regenerate and the stability would approach to the one achieved with the  $250^\circ\text{C}$  treatment of equal length.

Also the recent theory of Sio et al. [21], questioning the existence of the precursor reservoir, could explain the observations of Fig. 9. As described in the introduction (Sec. 1) in more detail, Sio et al. [21] suggested that the complicated behavior of LeTID during illuminated annealing on the one hand and dark annealing on the other hand could be explained by two different reaction pathways that also involve reverse reactions. The first, so-called light-soaking pathway would correspond to the typical degradation-regeneration behavior observed under illumination at elevated temperatures. The second, slower reaction pathway would be responsible for the degradation/recovery observed in dark-annealing conditions. Importantly, in addition to the forward reaction of the dark-annealing (the 2nd) pathway, dark annealing would also activate reverse reactions of the light-soaking pathway. Hence, explaining the results of Fig. 9 with this theory would require that the stabilization at  $265^\circ\text{C}$  derives mainly from the forward reaction of LeTID through the light-soaking pathway to the regenerated state (not necessarily related to H out-diffusion according to Sio et al. [21]), whereas the higher temperature during HIIT at  $370^\circ\text{C}$  would prevent fast regeneration by promoting the reverse reaction of the light-soaking pathway towards the precursor states. This reverse reaction could explain why the short 12 s HIIT processes at and above  $\sim 350^\circ\text{C}$  in Figs. 7–9 do not result in significant stabilization, and also why short dark anneals (e.g. 20 s at  $320^\circ\text{C}$  in Fig. 11 and 1 min at  $300^\circ\text{C}$  in Ref. [21]) result in destabilization of samples. Importantly, the mentioned theory also allows conjecturing why HIIT at  $370^\circ\text{C}$  in Figs. 7–9 eventually, after several minutes, results in stabilization. However, this stabilization would not occur through the forward-reaction pathway of LeTID regeneration but through the slow dark-annealing pathway (despite the presence of a high concentration of excess charge carriers): by removal of defects through e.g. hydrogen out-diffusion enabled by the high process temperature.

The consistency of the above defect removal/out-diffusion hypothesis can be reflected based on experimental results presented by Sio et al. [21]. According to effective lifetime vs. dark-annealing time curves of the mentioned study (Fig. 1 (b) in Ref. [21]), dark annealing as-fired p-type mono-like implied- $V_{oc}$  samples at  $240^\circ\text{C}$  results in degradation at the timescale of tens of minutes and subsequent recovery lasting hundreds of minutes, both presumably through the dark-annealing pathway. When the dark-annealing temperature is increased to  $300^\circ\text{C}$ , the degradation accelerates to the timescale of minutes while recovery occurs mostly within tens of minutes. Increasing the dark-annealing temperature even further to  $400^\circ\text{C}$  eliminates the degradation phase but still results in a distinct recovery phase that is a further order of magnitude faster compared to the dark anneal at  $300^\circ\text{C}$ . Hence, at  $400^\circ\text{C}$ , the majority of the recovery phase occurs already within minutes. On the other hand, when Sio et al. [21] prolonged the duration of a dark anneal at  $300^\circ\text{C}$  from 1 min to 100 min, they observed that instead of an increase in the defect concentration of LeTID during subsequent light soaking, a significant reduction, i.e. a stabilizing effect, can be achieved. Extrapolating this to the reactions through the

dark-anneal pathway at 400 °C, it seems plausible that a similar stabilization effect as achieved in 100 min at 300 °C through defect removal/out-diffusion could be reached already an order of magnitude faster at 400 °C, i.e. within 10 min or even less.

Assuming the premises of the model of Sio et al. [21] and comparing the above dark-annealing timescales to the treatment duration of 3 min that was necessary in Fig. 9 to achieve notable stabilization with HIIT at 370 °C, it seems possible that this process duration and temperature could promote the reactions of the dark-anneal pathway significantly. Therefore, LeTID stabilization would occur even if these high-temperature conditions would be unfavorable for the regeneration reaction through the light-soaking pathway. The fact that the stability after HIIT at such high temperatures in Fig. 8 is practically independent of the illumination intensity can be seen to support this hypothesis. On the other hand, such dark anneal-induced out-diffusion/defect passivation would take several hundred minutes at 265 °C. Therefore, the significant stabilization achieved with HIIT at 265 °C already in less than 60 s in Fig. 9 would be more likely to follow from the forward (regeneration) reaction of the LeTID defect through the light-soaking pathway. Hence, within the framework of this theory, only HIIT at 265 °C would result in LeTID regeneration typical to many light-soaking experiments in the literature, whereas HIIT at 370 °C would be effectively equivalent to dark annealing due to the high process temperature, despite the high concentration of excess carriers present during this process.

Although still hypotheses for now, the involvement of dark anneal-related reactions could provide an explanation for the complicated temperature dependence of Figs. 7–11 regardless of whether they relate to the increased rate of reverse reactions at high temperatures, the release of precursors from a reservoir, or the alternative dark-anneal pathway of the LeTID defect mechanism according to the model of Sio et al. [21]. It is also noteworthy that the overlap observed in Fig. 11 between the sample that was separately dark annealed at 320 °C for 20 s after HIIT at 52 kW/m<sup>2</sup> and 250 °C for 12 s and the sample HIIT processed at 52 kW/m<sup>2</sup> and 300 °C for 12 s can be seen to be consistent with theories involving dark-annealing phenomena. For example, in the framework of the 4-state theory, although the regeneration rate during HIIT at 300 °C would be equal or even higher than during HIIT at 250 °C, the higher temperature could introduce additional precursors from the reservoir state to an amount that is approximately comparable to the extra concentration of precursors released during the dark anneal at 320 °C for 20 s. This extra concentration of precursors after HIIT at 300 °C compared to HIIT at 250 °C would then be responsible for the more pronounced degradation during the LeTID test. On the other hand, within the theory of Sio et al. [21], the dark-anneal-associated reverse defect reactions of the light-soaking pathway could equally explain such overlap.

### 3.8. Implications of the temperature dependencies of HIIT on fast regeneration of LeTID

Although the short HIIT processes of this work that can be considered inline compatible (12 s–60 s) result in significant stabilization of LeTID especially at process temperatures around 250 °C, full stability is yet to be reached (compare e.g. the 12 s–60 s and the 10 min HIIT in Fig. 9). Regardless of the origin of the high-temperature instabilities discussed above, they limit the practical useable temperature range of industrial post-firing HIIT targeted for a short inline process. These instabilities (due to a precursor reservoir or another destabilization mechanism) mean that an acceleration of HIIT by increasing the process temperature to > 300 °C is not an attractive option since a process duration on the order of minutes is required to achieve a reasonable LeTID stability (as seen e.g. in Fig. 9). On the other hand, based on both Ref. [44] and Fig. 6, 250 °C is the lowest process temperature of this work that does not involve a typical degradation-regeneration cycle during the HIIT itself. Lower process temperatures, e.g. at 190 °C, involve a degradation-regeneration sequence, which for example in the case of the mc-Si

*iV<sub>oc</sub>* sample of Fig. 6 takes several minutes to complete. Although the samples are relatively stable after such full cycling (as seen e.g. in Fig. 8), a process duration of several minutes is likely too long for inline HIIT aimed at an industrial-scale throughput. This behavior represents a dilemma for using temperature adjustments for further improvement of the effectiveness of HIIT to promote the goal of using this method as a sole fast inline-compatible solution against LeTID.

A further approach to increase the effectiveness of HIIT could be to combine it with one or several pretreatment methods. For example, a second firing at 565 °C before HIIT was observed to improve the efficiency of LeTID stabilization in *iV<sub>oc</sub>* samples [25]. However, as already mentioned in Sec. 1, post-firing temperature steps above 450 °C have been found to lead to contact resistance degradation, and are therefore not directly useable on solar cells with fired metallization contacts [32]. Although such degradation was recently observed to be recoverable by a second anneal step, this adds to the complexity and the total duration of the post-firing processing steps [27]. Alternatively, such anneals can also be performed before firing, which was recently found to lead to a notable decrease of LeTID in symmetric HP mc-Si lifetime samples, hypothesized to derive from the removal of excess hydrogen from the bulk by effusion [28]. Whether such anneals could also be useful for improving the efficiency of HIIT as fast pretreatments through the removal of hydrogen or some other mechanism represents an interesting research question for the future.

### 3.9. Degradation of implied *V<sub>oc</sub>* after optimal HIIT

Although stabilizing as-fired mc-Si samples fully in an inline-compatible timescale seems challenging with HIIT alone, these processes are still likely to provide a notable improvement of the energy yield during the expected operating lifetime of solar modules in the field. In this section, we estimate the magnitude of the yield improvements after HIIT in comparison to non-treated references. In addition, based on the results of the above sections, we sketch a compromise treatment intended to combine as high stability as possible with a treatment time that is still compatible with an industrial-scale inline process.

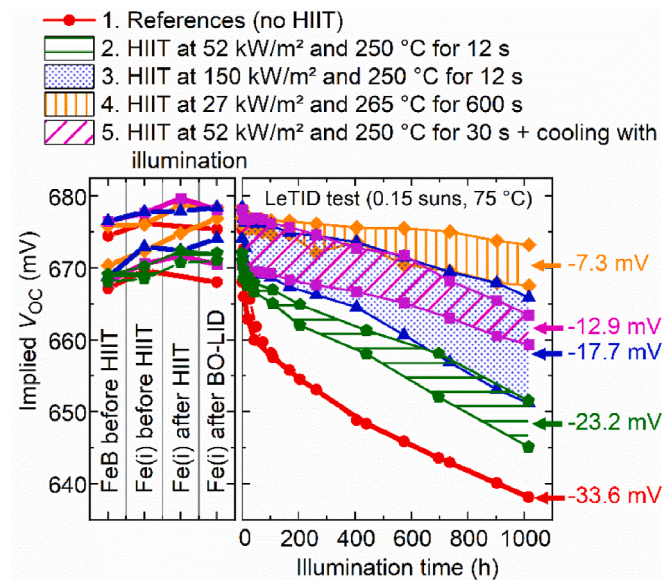


**Fig. 12.** Comparison of *iV<sub>oc</sub>* degradation during the LeTID test after the optimal HIIT processes of this work. Non-treated references are included for comparison (red dotted curves). Indicated on the right is the average *iV<sub>oc</sub>* loss for each treatment after 1000 h of LeTID testing. The shadowed areas correspond to the difference of two different identically processed samples. (For interpretation of the references to color in this figure legend, the reader is referred to the Web version of this article.)

As a practical measure of degradation after HIIT, Fig. 12 compares selected treatments in terms of 1-sun  $iV_{oc}$  degradation during the 1000 h LeTID test. These treatments include the optimum air-cooled and water-cooled processes at  $52 \text{ kW/m}^2$  and  $150 \text{ kW/m}^2$ , respectively, both at  $250^\circ\text{C}$  for 12 s (see Fig. 7). These are compared to both non-treated references and the most stable long process of this work at  $27 \text{ kW/m}^2$  and  $265^\circ\text{C}$  for 600 s (see Fig. 9). In addition, we added a new process that in terms of the process intensity and temperature corresponds to the optimum treatment with air cooling in Fig. 7 ( $52 \text{ kW/m}^2$  and  $250^\circ\text{C}$ ). However, we extended its duration to 30 s which could still be a feasible duration for an air-cooled inline tool without compromising excessively on throughput or factory footprint. Further, since applying illumination during the cooling ramp had a favorable effect on the stability in Fig. 10, the cooling from the last mentioned 30 s process was performed under  $1.5 \text{ kW/m}^2$  intensity for 15 s as described in section 3.6.

Based on Fig. 12, the stability of the HIIT process at  $52 \text{ kW/m}^2$  and  $250^\circ\text{C}$  for 12 s is still quite far from the long treatment at  $27 \text{ kW/m}^2$  and  $265^\circ\text{C}$  for 600 s which results in considerable stabilization within the 1000 h LeTID testing time. The stability improves by increasing the intensity to  $150 \text{ kW/m}^2$  with liquid cooling. However, as liquid cooling complicates the design of the inline tool, it may be a reasonable compromise to prolong the duration of the air-cooled treatment at  $52 \text{ kW/m}^2$  and  $250^\circ\text{C}$  to 30 s. This, combined with illumination during the cooling ramp from the process temperature, results in a stability that is comparable to or even slightly better than that of the high-intensity process at  $150 \text{ kW/m}^2$  and  $250^\circ\text{C}$  for 12 s, reducing the  $iV_{oc}$  loss after the 1000 h LeTID test by  $\sim 60\%$  as compared to the non-treated references.

In addition to the 1-sun  $iV_{oc}$  data of Fig. 12, injection-dependent lifetime data obtained with the QSSPC method also allow the evaluation of the implied current density and voltage at the maximum power point at 1 sun. By integrating this data with respect to the LeTID testing time, it is possible to obtain a rough estimation of the energy yield loss due to LeTID after the different HIIT treatments of Fig. 12. Hence, the fraction of the original yield loss of the references that can be avoided by applying these treatments can be calculated. Table 2 lists average values of these quantities based on two different samples per treatment.

Based on the results of Table 2, the energy yield loss due to LeTID reduces from 5.4% down to less than 2% during the 1000 h LeTID test by applying the optimum HIIT processes of this work. This corresponds to up to a 65% reduction in energy lost to LeTID. Although the largest decrease results from the long process at  $27 \text{ kW/m}^2$  and  $265^\circ\text{C}$  for 600 s, the difference compared to the process at  $52 \text{ kW/m}^2$  and  $250^\circ\text{C}$  for 30 s with illumination during the cooling ramp is very small in terms of the expected yield loss. Hence, efficient HIIT leading to a substantial

**Table 2**

Relative energy yield loss due to LeTID during the 1000 h test after the HIIT processes of Fig. 12. The estimation is based on the implied current density and voltage at the maximum power point at 1 sun, obtained from injection-dependent QSSPC data. The relative loss is in reference to a hypothetical yield in the case that the samples would not degrade from their state “Fe(i) after BO-LID” anymore. Further, relative yield loss reductions, compared to the yield loss of the references due to LeTID, are shown for each treatment. All values correspond to an average of two similarly treated samples.

No. in Fig. 12	1.	2.	3.	4.	5.
Intensity ( $\text{kW/m}^2$ )	Ref.	52	150	27	52
Temperature ( $^\circ\text{C}$ )		250	250	265	250
Treatment time (s)		12	12	600	30
Cooling condition		Dark	Dark	Dark	Illuminated
$iV_{oc}$ loss after the 1000 h LeTID test	33.6 mV	23.2 mV	17.7 mV	7.3 mV	12.9 mV
Relative energy yield loss due to LeTID	5.4%	3.9%	2.9%	1.9%	2.0%
Relative yield loss reduction compared to Ref.	0%	28%	46%	65%	63%

improvement of the energy yield of the treated solar cells is obtainable with an air-cooled tool in an inline-feasible timescale.

#### 4. Conclusions

In this work, we have evaluated the inline feasibility of high-intensity illumination treatments (HIIT) against LeTID by applying a wide process parameter variation mainly within the operating range reachable with air cooling. These treatments were followed by a stability test at 0.15 suns and  $75^\circ\text{C}$  for 1000 h. These conditions were found to induce degradation of the effective lifetime in the bulk, whereas  $J_{0,\text{surface}}$  analysis revealed no surface-related degradation. The results show that the stability improves with increasing treatment intensity up to  $150 \text{ kW/m}^2$ , but also that increasing the temperature from an optimum range at  $250^\circ\text{C}$  leads to a substantial decrease of stability in the case of short treatments. However, prolonging the treatment time to minutes evens out these stability differences between the different treatment temperatures.

To understand the role of conditions during the cooling ramp from the HIIT temperature in the above process temperature-dependent behavior of LeTID stability, we cooled samples both in the dark and under illumination. Further, a separate dark annealing was performed after HIIT. Here, it was found that illumination during cooling improves the stability, which is most likely attributable to an additional regeneration effect during the illuminated cooling. Notably, especially the results of the separate dark annealing experiment suggest that the stability differences between the different HIIT temperatures are more likely attributable to reactions at the treatment conditions themselves than to those during the cooling ramp in the dark.

The results were discussed based on both three- and four-state defect models of LeTID, as well as a recently introduced model of Sio et al. [21] involving two separate defects and reaction pathways under light soaking on the one hand and during dark annealing on the other hand. A feasible explanation for the results is that the high-temperature treatments induce effects that have previously been associated with dark-annealing experiments. For example, a substantially more pronounced release of precursors from a reservoir state could occur during HIIT at high temperatures  $> 300^\circ\text{C}$  than at more optimal lower temperatures. The eventual depletion of this reservoir after several minutes would then result in stabilization also at the high temperatures, so that the stability approaches that achieved with the optimum temperature treatments. Alternatively, assuming two different reaction paths for light soaking and dark annealing, HIIT at too high temperatures could promote the reverse reaction of the light-soaking pathway of LeTID together with the slow forward reaction of the dark-anneal pathway. These reactions would also eventually lead to stabilization through defect removal/passivation by e.g. out-diffusion of hydrogen. Regardless of their origin, the observed temperature dependences pose practical restrictions to the parameter range available for rapid inline post-firing HIIT, which limit the minimum duration at which reasonable stabilization of LeTID can be reached.

To investigate the practical benefits of HIIT, 1-sun implied  $V_{oc}$  and estimated energy yield losses due to LeTID after the best treatments found in the study were compared to non-treated references. While considerable improvement of stability was obtained in only 12 s, an optimized 30 s process with illumination applied also during the cooling ramp from the process temperature resulted in a comparable stability as a long 10 min process. Hence, the energy yield loss due to LeTID can be reduced by up to over 60% as compared to non-treated references in an inline-feasible timescale. At present, the results presented in this work apply to climate conditions equivalent to Central Europe, and further work is necessary for a generalization to notably warmer climates.

#### CRediT authorship contribution statement

Henri Vahlman: Conceptualization, Experiment planning, Sample

design and processing, Experimental execution, Manuscript – structuring and writing, Visualization. **Sebastian Roder:** Conceptualization, Development of HIIT-regeneration tool, Experimental execution, Writing, Visualization. **Jan Nekarda:** Funding acquisition, Project administration. **Stefan Rein:** Conceptualization, Experiment planning and support, Funding acquisition, Project administration.

## Declaration of competing interest

The authors declare that they have no known competing financial interests or personal relationships that could have appeared to influence the work reported in this paper.

## Acknowledgements

This work was funded by the German Federal Ministry for Economic Affairs and Energy with the project UFO under contract number 0324080B.

The authors acknowledge Dr. Wolfram Kwapil for valuable discussions and recommendations during manuscript writing.

## References

- [1] K. Bothe, R. Sinton, J. Schmidt, Fundamental boron-oxygen-related carrier lifetime limit in mono- and multicrystalline silicon, *Prog. Photovoltaics Res. Appl.* 13 (2005) 287, <https://doi.org/10.1002/pip.586>.
- [2] F. Kersten, P. Engelhart, H.-C. Ploigt, A. Stekolnikov, T. Lindner, F. Stenzel, M. Bartzsch, A. Szpeth, K. Petter, J. Heitmann, J.W. Müller, Degradation of multicrystalline silicon solar cells and modules after illumination at elevated temperature, *Sol. Energy Mater. Sol. Cell.* 142 (2015) 83–86, <https://doi.org/10.1016/j.solmat.2015.06.015>.
- [3] K. Ramspeck, S. Zimmermann, H. Nagel, A. Metz, Y. Gassenbauer, B. Birkmann, A. Seidl, Light Induced Degradation of Rear Passivated Mc-Si Solar Cells, Proceedings of 27th European Photovoltaic Solar Energy Conference and Exhibition, Frankfurt, Germany, 2012, pp. 861–865, <https://doi.org/10.4229/27EUPVSEC2012-2DO.3.4>.
- [4] F. Fertig, K. Krauß, S. Rein, Light-induced degradation of PECVD aluminium oxide passivated silicon solar cells, *Phys. Status Solidi RRL* 9 (2015) 41–46, <https://doi.org/10.1002/psrr.20140942>.
- [5] A.A. Brand, K. Krauß, P. Wild, S. Schörner, S. Gutscher, S. Roder, S. Rein, J. Nekarda, Ultrafast In-Line Capable Regeneration Process for Preventing Light Induced Degradation of Boron-Doped P-type Cz-Silicon PERC Solar Cells, 33rd European Photovoltaic Solar Energy Conference and Exhibition, Amsterdam, Netherlands, 2017, pp. 382–387, <https://doi.org/10.4229/EUPVSEC20172017-2CO.9.5>.
- [6] F. Fertig, R. Lantzsch, A. Mohr, M. Schaper, M. Bartzsch, D. Wissen, F. Kersten, A. Mette, S. Peters, A. Eidner, J. Cieslak, K. Duncker, M. Junghänel, E. Jarzembski, M. Kauert, B. Faulwetter-Quandt, D. Meißner, B. Reiche, S. Geißler, S. Hörmlein, C. Klenke, L. Niebergall, A. Schönmann, A. Weirauch, F. Stenzel, A. Hofmann, T. Rudolph, A. Schwabedissen, M. Gundermann, M. Fischer, J.W. Müller, D.J.W. Jeong, Mass production of p-type Cz silicon solar cells approaching average stable conversion efficiencies of 22 %, *Energy Procedia* 124 (2017) 338–345, <https://doi.org/10.1016/j.egypro.2017.09.308>.
- [7] K. Petter, K. Hübener, F. Kersten, M. Bartzsch, F. Fertig, J. Müller, Dependence of LeTID on brick height for different wafer suppliers with several resistivities and dopants, *Proceedings of 9th Int. Workshop Cryst. Silicon Sol. Cells* (2016).
- [8] H. Vahlman, M. Wagner, F. Wolny, A. Krause, H. Laine, A. Ingolese, M. Yli-Koski, H. Savin, Light-induced degradation in quasi-monocrystalline silicon PERC solar cells: indications on involvement of copper, *Phys. Status Solidi* 214 (2017), <https://doi.org/10.1002/pssa.201700321>.
- [9] D. Chen, P.G. Hamer, M. Kim, G. Bourret-Sicotte, S. Liu, A. Ciesla, C.E. Chan, R. Chen, T.H. Fung, C. Vargas, Q. Ye, M.D. Abbott, B.J. Hallam, S.R. Wenham, Hydrogen induced degradation a possible mechanism for light- and elevated temperature-induced degradation in n-type silicon, *Sol. Energy Mater. Sol. Cell.* 185 (2018) 174–182, <https://doi.org/10.1016/j.solmat.2018.05.034>.
- [10] J.M. Fritz, A. Zuschlag, D. Skorka, A. Schmid, G. Hahn, Temperature dependent degradation and regeneration of differently doped mc-Si materials, *Energy Procedia* 124 (2017) 718–725, <https://doi.org/10.1016/j.egypro.2017.09.085>.
- [11] D. Bredemeier, D.C. Walter, J. Schmidt, Lifetime degradation in multicrystalline silicon under illumination at elevated temperature: indications for the involvement of hydrogen, *AIP Conference Proceedings* 1999 (2018) 130001, <https://doi.org/10.1063/1.5049320>.
- [12] C. Vargas, K. Kim, G. Coletti, D. Payne, C. Chan, S. Wenham, Z. Hameiri, Carrier-induced degradation in multicrystalline silicon: dependence on the silicon nitride passivation layer and hydrogen released during firing, *IEEE Journal of Photovoltaics* 8 (2018) 413–420, <https://doi.org/10.1109/JPHOTOV.2017.2783851>.
- [13] T. Niewelt, F. Schindler, W. Kwapil, R. Eberle, J. Schön, M.C. Schubert, Understanding the light-induced degradation at elevated temperatures: similarities between multicrystalline and floatzone p-type silicon, *Prog. Photovoltaics Res. Appl.* 26 (2018) 533–542, <https://doi.org/10.1002/pip.2954>.
- [14] A. Herguth, P. Keller, N. Mundhaas, Influence of temperature on light induced phenomena in multicrystalline silicon, *AIP Conference Proceedings* 1999 (2018) 130007, <https://doi.org/10.1063/1.5049326>.
- [15] T.H. Fung, M. Kim, D. Chen, A. Samadi, C.E. Chan, B.J. Hallam, S. Wenham, M. Abbott, Influence of bound hydrogen states on carrier-induced degradation in multi-crystalline silicon, *AIP Conference Proceedings* 1999 (2018) 130004, <https://doi.org/10.1063/1.5049323>.
- [16] J. Schmidt, D. Bredemeier, D.C. Walter, On the defect physics behind light and elevated temperature-induced degradation (LeTID) of multicrystalline silicon solar cells, *IEEE Journal of Photovoltaics* 9 (2019) 1497–1503, <https://doi.org/10.1109/JPHOTOV.2019.2937223>.
- [17] K. Nakayashiki, J. Hofstetter, A.E. Morishige, T.-T.A. Li, D.B. Needleman, M. A. Jensen, T. Buonassisi, Engineering solutions and root-cause analysis for light-induced degradation in p-type multicrystalline silicon PERC modules, *IEEE Journal of Photovoltaics* 6 (2016) 860–868, <https://doi.org/10.1109/JPHOTOV.2016.2556981>.
- [18] T. Luka, S. Großer, C. Hagendorf, K. Ramspeck, M. Turek, Intra-grain versus grain boundary degradation due to illumination and annealing behavior of multi-crystalline solar cells, *Sol. Energy Mater. Sol. Cell.* 158 (2016) 43–49, <https://doi.org/10.1016/j.solmat.2016.05.061>.
- [19] A. Herguth, C. Derrick, P. Keller, B. Terheiden, Recovery of LeTID by low intensity illumination: reaction kinetics, completeness and threshold temperature, *Energy Procedia* 124 (2017) 740–744, <https://doi.org/10.1016/j.egypro.2017.09.090>.
- [20] T.H. Fung, M. Kim, D. Chen, C.E. Chan, B.J. Hallam, R. Chen, D.N.R. Payne, A. Ciesla, S.R. Wenham, M.D. Abbott, A four-state kinetic model for the carrier-induced degradation in multicrystalline silicon: introducing the reservoir state, *Sol. Energy Mater. Sol. Cell.* 184 (2018) 48–56, <https://doi.org/10.1016/j.solmat.2018.04.024>.
- [21] H.C. Sio, D. Kang, X. Zhang, J. Yang, J. Jin, D. Macdonald, The role of dark annealing in light and elevated temperature induced degradation in p-type mono-like silicon, *IEEE Journal of Photovoltaics* 10 (2020) 992–1000, <https://doi.org/10.1109/JPHOTOV.2020.2993653>.
- [22] M. Yli-Koski, M. Serué, C. Modanese, H. Vahlman, H. Savin, Low-temperature dark anneal as pre-treatment for LeTID in multicrystalline silicon, *Sol. Energy Mater. Sol. Cell.* 192 (2019) 134–139, <https://doi.org/10.1016/j.solmat.2018.12.021>.
- [23] R. Sharma, A.G. Aberle, J.B. Li, Optimization of belt furnace anneal to reduce light and elevated temperature induced degradation of effective carrier lifetime of P-type multicrystalline silicon wafers, *Sol. RRL Solar* 2 (2018) 1800070, <https://doi.org/10.1002/solr.201800070>.
- [24] R. Eberle, W. Kwapil, F. Schindler, S.W. Glunz, M.C. Schubert, Firing temperature profile impact on light induced degradation in multicrystalline silicon, *Energy Procedia* 124 (2017) 712–717, <https://doi.org/10.1016/j.egypro.2017.09.082>.
- [25] C.E. Chan, D.N.R. Payne, B.J. Hallam, M.D. Abbott, T.H. Fung, A.M. Wenham, B. S. Tjajhono, S.R. Wenham, Rapid stabilization of high-performance multicrystalline P-type silicon PERC cells, *IEEE Journal of Photovoltaics* 6 (2016) 1473–1479, <https://doi.org/10.1109/JPHOTOV.2016.2606704>.
- [26] C. Sen, M. Kim, D. Chen, U. Varshney, S. Liu, A. Samadi, A. Ciesla, S.R. Wenham, C. E. Chan, C. Chong, M.D. Abbott, B.J. Hallam, Assessing the impact of thermal profiles on the elimination of light- and elevated-temperature-induced degradation, *IEEE Journal of Photovoltaics* 9 (2019) 40–49, <https://doi.org/10.1109/JPHOTOV.2018.2874769>.
- [27] C. Sen, C. Chan, P. Hamer, M. Wright, C. Chong, B. Hallam, M. Abbott, Eliminating light- and elevated temperature-induced degradation in P-type PERC solar cells by a two-step thermal process, *Sol. Energy Mater. Sol. Cell.* 209 (2020) 110470, <https://doi.org/10.1016/j.solmat.2020.110470>.
- [28] C. Sen, C. Chan, P. Hamer, M. Wright, U. Varshney, S. Liu, D. Chen, A. Samadi, A. Ciesla, C. Chong, B. Hallam, M. Abbott, Annealing prior to contact firing: a potential new approach to suppress LeTID, *Sol. Energy Mater. Sol. Cell.* 200 (2019) 109938, <https://doi.org/10.1016/j.solmat.2019.109938>.
- [29] D.N.R. Payne, C.E. Chan, B.J. Hallam, B. Hoex, M.D. Abbott, S.R. Wenham, D. M. Bagnall, Rapid passivation of carrier-induced defects in p-type multi-crystalline silicon, *Sol. Energy Mater. Sol. Cell.* 158 (2016) 102–106, <https://doi.org/10.1016/j.solmat.2016.05.022>.
- [30] D.N.R. Payne, C.E. Chan, B.J. Hallam, B. Hoex, M.D. Abbott, S.R. Wenham, D. M. Bagnall, Acceleration and mitigation of carrier-induced degradation in p-type multi-crystalline silicon, *Phys. Status Solidi RRL* 10 (2016) 237–241, <https://doi.org/10.1002/psrr.201510437>.
- [31] K. Krauß, A.A. Brand, F. Fertig, S. Rein, J. Nekarda, Fast regeneration processes to avoid light-induced degradation in multicrystalline silicon solar cells, *IEEE Journal of Photovoltaics* 6 (2016) 1427–1431, <https://doi.org/10.1109/JPHOTOV.2016.2598273>.
- [32] C. Chan, P. Hamer, G. Bourret-Sicotte, R. Chen, A. Ciesla, B. Hallam, D. Payne, R. S. Bonilla, S. Wenham, Instability of increased contact resistance in silicon solar cells following post-firing thermal processes, *Sol. RRL* 1 (2017) 1700129, <https://doi.org/10.1002/solr.201700129>.
- [33] C. Chan, T.H. Fung, M. Abbott, D. Payne, A. Wenham, B. Hallam, R. Chen, S. Wenham, Modulation of carrier-induced defect kinetics in multi-crystalline silicon PERC cells through dark annealing, *Sol. RRL* 1 (2017) 1600028, <https://doi.org/10.1002/solr.201600028>.
- [34] S. Liu, D. Payne, C. Vargas Castrillon, D. Chen, M. Kim, C. Sen, U. Varshney, Z. Hameiri, C. Chan, M. Abbott, S. Wenham, Impact of dark annealing on the kinetics of light- and elevated-temperature-induced degradation, *IEEE Journal of Photovoltaics* 8 (2018) 1494–1502, <https://doi.org/10.1109/JPHOTOV.2018.2866325>.

- [35] A. Herguth, A. Graf, G. Hahn, On the Influence of Advection Cooling during Degradation and Regeneration of Boron-Oxygen Defects Using High Intensities, Proceedings of 36th European Photovoltaic Solar Energy Conference and Exhibition, Marseille, France, 2019, pp. 116–119, <https://doi.org/10.4229/EUPVSEC20192019-2AO.4.5>.
- [36] C. Möller, T. Bartel, F. Gibaja, K. Lauer, Iron-boron pairing kinetics in illuminated p-type and in boron/phosphorus co-doped n-type silicon, *J. Appl. Phys.* 116 (2014) 24503, <https://doi.org/10.1063/1.4889817>.
- [37] A. Kimmerle, J. Greulich, A. Wolf, Carrier-diffusion corrected  $J_0$ -analysis of charge carrier lifetime measurements for increased consistency, *Sol. Energy Mater. Sol. Cell.* 142 (2015) 116–122, <https://doi.org/10.1016/j.solmat.2015.06.043>.
- [38] S. Wilking, J. Engelhardt, S. Ebert, C. Beckh, A. Herguth, G. Hahn, High Speed Regeneration of BO-Defects: Improving Long-Term Solar Cell Performance within Seconds, 29th European Photovoltaic Solar Energy Conference and Exhibition, Amsterdam, Netherlands, 2014, pp. 366–372, <https://doi.org/10.4229/EUPVSEC20142014-2BP.1.2>.
- [39] D. Sperber, A. Graf, D. Skorka, A. Herguth, G. Hahn, Degradation of surface passivation on crystalline silicon and its impact on light-induced degradation experiments, *IEEE Journal of Photovoltaics* 7 (2017) 1627–1634, <https://doi.org/10.1109/JPHOTOV.2017.2755072>.
- [40] D. Sperber, A. Schwarz, A. Herguth, G. Hahn, Bulk and surface-related degradation in lifetime samples made of czochralski silicon passivated by plasma-enhanced chemical vapor deposited layer stacks, *Phys. Status Solidi* 215 (2018) 1800741, <https://doi.org/10.1002/pssa.201800741>.
- [41] K.R. McIntosh, L.E. Black, On effective surface recombination parameters, *J. Appl. Phys.* 116 (2014) 14503, <https://doi.org/10.1063/1.4886595>.
- [42] A. Herguth, On the lifetime-equivalent defect density: properties, application, and pitfalls, *IEEE Journal of Photovoltaics* 9 (2019) 1182–1194, <https://doi.org/10.1109/JPHOTOV.2019.2922470>.
- [43] H. Vahlman, S. Roder, K. Krauß, J. Nekarda, S. Rein, Evaluation of Inline High-Intensity Illumination Treatments against LeTID, 37rd European Photovoltaic Solar Energy Conference and Exhibition, 2020, pp. 409–413, <https://doi.org/10.4229/EUPVSEC20202020-2CV.1.56>, online.
- [44] S. Liu, C. Chan, D. Chen, M. Kim, C. Sen, U. Varshney, B. Hallam, M. Abbott, S. Wenham, D. Payne, Investigation of temperature and illumination dependencies of carrier-induced degradation in p-type multi-crystalline silicon, *AIP Conference Proceedings* 1999 (2018) 130014, <https://doi.org/10.1063/1.5049333>.
- [45] E. Seifert, OriginPro 9.1: scientific data analysis and graphing software-software review, *J. Chem. Inf. Model.* 54 (2014) 1552, <https://doi.org/10.1021/ci500161d>.